



## FUSION OF MODELING AND REMOTE SENSING FOR DAMAGE ESTIMATION

L. Moya<sup>(1,2)</sup>, E. Mas<sup>(3)</sup>, S. Koshimura<sup>(4)</sup>, F. Yamazaki<sup>(5)</sup>, W. Liu<sup>(6)</sup>, C. Geiß<sup>(7)</sup>

<sup>(1)</sup> Researcher, IRIDeS, Tohoku University, Japan, [lmoyah@irides.tohoku.ac.jp](mailto:lmoyah@irides.tohoku.ac.jp)

<sup>(2)</sup> Principal Investigator, CISMID, National University of Engineering, Peru, [lmoyah@uni.pe](mailto:lmoyah@uni.pe)

<sup>(3)</sup> Associate Professor, IRIDeS, Tohoku University, Japan, [mas@irides.tohoku.ac.jp](mailto:mas@irides.tohoku.ac.jp)

<sup>(4)</sup> Professor, IRIDeS, Tohoku University, Japan, [koshimura@irides.tohoku.ac.jp](mailto:koshimura@irides.tohoku.ac.jp)

<sup>(5)</sup> Research Fellow, National Research Institute for Earth Science and Disaster Resilience, Japan, [fumio.yamazaki@bosai.go.jp](mailto:fumio.yamazaki@bosai.go.jp)

<sup>(6)</sup> Assistant Professor, Graduate School of Engineering, Chiba University, [wen.liu@chiba-u.jp](mailto:wen.liu@chiba-u.jp)

<sup>(7)</sup> Researcher, German Remote Sensing Data Center, German Aerospace Center, [Christian.Geiss@dlr.de](mailto:Christian.Geiss@dlr.de)

### Abstract

Disaster risk analysis involves a set of disaster events, their consequences, and their probabilities of occurrence over a defined period. The main, or traditional role of disaster risk is to serve as a guide for decisions about safety. Whether the infrastructure requires retrofitting or whether having insurance is cost-effective are such examples. An important stage in estimating the disaster risk is the estimation of damage as a function of the demand (i.e., ground motion for earthquake or inundation depth for tsunamis). These damage functions have been playing the main role in one of the recent trends. With the technological progress in instrumentation, numerical modeling and communication networks, in the aftermath of a large-scale disaster, it is possible to estimate a demand map in real/near-real time. Then, with the aid of the damage functions, an estimation of the damage map can be computed. However, with damage functions, we can only compute the probability that an asset is damaged. The best that can be done with such information is to report the expected amount of damaged assets within a given area. It is not possible to indicate which asset was damaged. A more realistic estimation of damage due to an arbitrary disaster can be obtained from remote sensing data, such as satellite images. With remote sensing data recorded after a disaster (images recorded before a disaster are usually available as well), the real effect of the disaster can be detected. However, the procedure is not straightforward. Usually, a set of features are computed from remote sensing data for each asset. Such features are used as input of a *discriminant function* that predicts whether the asset is damaged or not. The discriminant function is best calibrated using machine learning methods, but they require training data. Training data is very difficult to collect right after a disaster because all the efforts are focused on rescue and relief activities. In this paper we summarize the studies we have performed regarding the fusion of the two referred disciplines to implement a fully automatic damage mapping procedure.

*Keywords: damage mapping, machine learning, damage functions, demand modeling.*



## 1. Introduction

The identification of damage to an urban area in the aftermath of a large-scale disaster is a critical work in emergency response and recovery activities. The more knowledge regarding the extent of affected areas, the better the decisions will be during the emergency. Currently, remote sensing is the main technology to retrieve the extent of the damage in the aftermath of a large-scale disaster [1]-[3]. The most efficient method to identify damage is the comparison of a pair of images recorded before (*pre-event*) and after (*post-event*) the disaster in mention, an approach usually referred to as *change detection*. If the acquisition date of both the pre-event and post-event images is close enough, changes observed between the images are assumed to be associated with the effects of the disaster. In order to identify changes, certain features are computed from the both images to measure the degree of similarity/change. The averaged pixel difference, the correlation coefficient, and the coherence are features frequently used. Among the tendencies to identify damage from remote sensing-based features is the search of *discriminant functions* that can produce damage maps with acceptable accuracy. Liu et al. [4] proposed a linear combination of the absolute value of the normalized difference of backscattering intensity and the correlation coefficient, introduced as *z-factor*, to discriminate changes between a pair of TerraSAR-X intensity images. Gokon et al. [5] proposed a damage function called  $F_{RM}$  that uses a mean value of correlation coefficient within an area defined by object-based analysis. It was later reported that the direct application of the *z-factor* and  $F_{RM}$  function in microwave images of different spectral bands was not possible, and recalibration was first needed [6][7]. Karimzadeh and Matsuoka [8] proposed a discriminant function whose inputs are the coherence and the averaged difference of backscattering intensity computed over different polarizations. However, the proposed function was calibrated independently for Sentinel-1 and ALOS-2 microwave imagery, and later on, it was calibrated for COSMO-SkyMed imagery [9]. It is observed that proposing a fixed discriminant function is strongly constrained to specific set of features and specific type of remote sensing data.

In order to overcome the pitfall referred above, the calibration of the discriminant function must be part of the processing-chain for damage mapping. Supervised machine learning algorithms were created for this kind of problem. Namely, supervised machine learning calibrates the discriminant function from limited but properly encoded *training data*. Wieland et al. [10] used the support vector machine (SVM) to calibrate discriminant functions from high-dimensional feature space and identified the affected area in Miyagi Prefecture due to the 2011 Tohoku earthquake-tsunami. Bai et al. [11] tested some deep neural networks for damage recognition using only a post-event microwave image. Moya et al. [12] used SVM to calibrate a discriminant function whose input is LiDAR-based features. Moya et al. [13] used SVM to calibrate a discriminant function whose input are three-dimensional texture features. Moya et al. [14] proposed a new feature, termed *conditional coherence*, and calibrated a discriminant function with one-class SVM that uses the conditional coherence as input to identify flooded areas in agricultural targets. As noted, the advantages of the use of machine learning algorithms is that (i) it is adaptable to arbitrary n-dimensional feature space, (ii) the type of sensor (i.e., microwave, optical, LiDAR data) is no longer relevant, and (iii) more complex discriminant function can be calibrated. However, supervised machine learning algorithms also exhibit a critical issue for damage mapping tasks: the need for training samples. The most accurate training data comes from field surveys, but in the aftermath of a large-scale disaster, the main efforts are focused on relief distribution and rescue activities. Usually, information regarding damage in the infrastructure is available after several weeks. Training data can be prepared from visual inspection of high-resolution optical images; however, it is time-consuming and may introduce biases. Most of the applications of machine learning algorithms referred previously used training data published many weeks, sometimes even months, after a certain disaster, and there are many more studies that exhibit the same issue. Namely, the use of training data that was not available right after the disaster. It is worth to point out that the scarce availability of training data has been observed in other applications of machine learning, and thus, some approaches have been proposed [15][16][17].

In the field of risk analysis, damage mapping is estimated from statistical studies of the relation between a demand parameter and the damage level of a building with specific properties (i.e., material, construction year, etc.) [18]-[21]. The demand parameter denotes the intensity of the disaster experienced at



certain geolocation. The peak ground acceleration for earthquakes and the inundation depth for tsunamis are such examples of demand parameters. A *fragility function* is the result of the referred statistical studies, and thus, it expresses the relationship between the demand parameter and the probability that a certain damage level is reached or exceeded [21]. Recently, several real-time building damage mapping in terms of probabilities has been implemented [22]-[25]. Part of the success of the referred frameworks lies on the progress in instrumentation and numerical modeling of the demand parameter [26]-[30]. The limitation of this approach is that it provides the probability of damage to a building, rather than its actual damage situation. It has been used, though, to provide local aggregates.

In this paper, we summarize our studies on the fusion of the two approaches, machine learning-remote sensing-based and probability-based damage mapping. We show that the fusion brings great benefits, such as the overcome of training data problem and the mapping of actual damage in near-real-time. The next chapter summarizes our first attempt of the fusion [31]. Chapter 3 reports the subsequent upgrade of the method [32]. Chapter 4 provides a glimpse of our current work. Finally, our conclusions are drawn in Chapter 5.

## 2. Replacing training data with demand parameters and damage functions

Instead of using training data to calibrate a discriminant function, the demand parameter and fragility functions are used to impose a novel constraint. Fig. 1 shows the processing chain of the proposed damage mapping method, and the steps are described as follows:

1. The satellite images are inserted into the system for a further analysis.
2. Feature extraction. Here the first database is prepared. The features are designed to detect changes between the pre-event and post-event images. The features are computed for each building to be analyzed. Fig. 1 shows a database with only two features (F1 and F2).
3. A discriminant function candidate is set. Fig. 1 shows a discriminant function drawn in the bi-dimensional space. The application of the function candidate on the feature database will create a damage scenario, hereafter referred to as the *synthetic scenario*.
4. An inventory of change/no-change samples is constructed from the synthetic scenario. Additionally, the demand parameter at each sample building is collected from the demand parameter map.
5. The samples are grouped into bins by ranges of the demand parameter. For each bin, the ratio of samples classified as changed ( $cr$ ) and the averaged demand parameter are computed. Then, the level of matching between  $cr$  and a fragility function is evaluated.

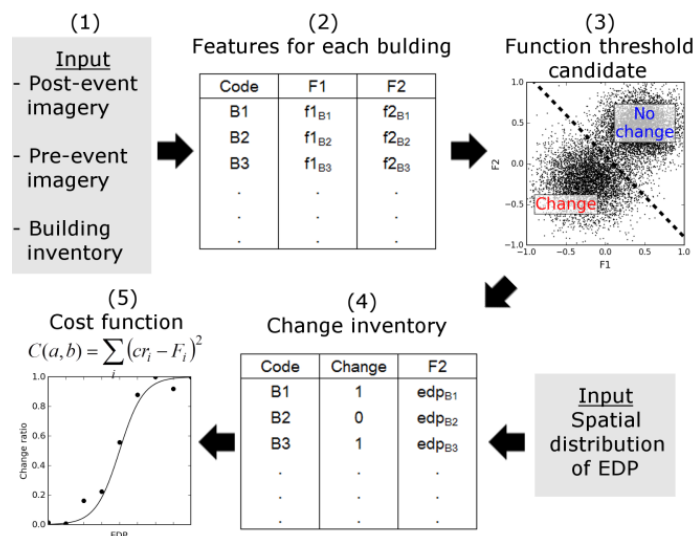


Fig. 1 – Schematic illustration of the flowchart of the proposed method. Source: [31].



The parameters of the discriminant function are searched through brute force repeating steps 3-5 over a range of potential values. The performance of the method was evaluated in the case of the 2011 Tohoku-Oki earthquake-tsunami. Fig. 2 depicts the demand parameter map (i.e., inundation depth in this case), the pre-event and post-event TerraSAR-X intensity images. Two features were computed from the images for each building: the correlation coefficient and the averaged difference of intensity. The proposed procedure was performed twice: one case using the fragility function proposed by Koshimura et al. [33], and the other case using the fragility function proposed by Supasri et al. [34]. Both fragility functions represent the relationship between the inundation depth and the probability that a building will be destroyed/washed away. In Fig. 3a, the solid blue lines represent the fragility functions used in the two cases, and the black points represent the  $cr$  values that best match the fragility functions. The bi-dimensional samples are shown in Fig 3b, from which the samples colored red are classified as destroyed and the samples colored blue were classified as non-destroyed. Fig. 4 shows a closer look of the destroyed building map from surveyed data and that estimated by the proposed method. The results achieved an overall accuracy of 81.4% and 84.9% using the fragility functions provided by Koshimura et al. [33] and Suppasri et al. [34], respectively. Further details of the proposed method can be found in [31].

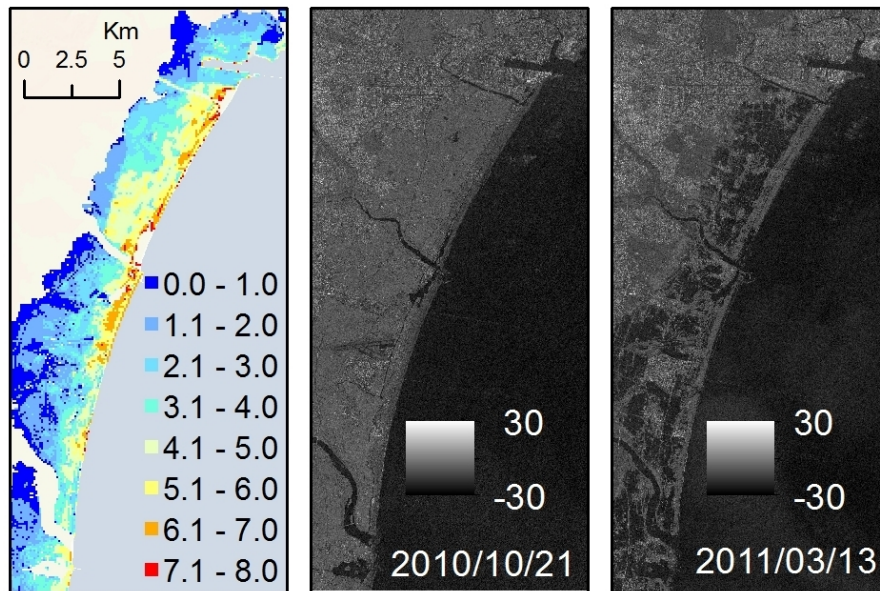


Fig. 2 – Input data. (left) demand parameter map (inundation depth); (center) pre-event TerraSAR-X intensity image; (right) post-event TerraSAR-X intensity image

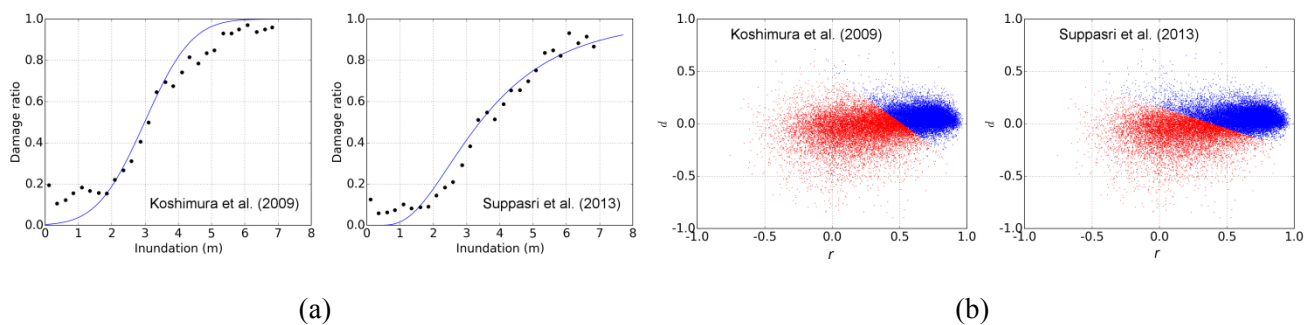


Fig. 3 – (a) Ratio of destroyed buildings vs. the inundation depth obtained from the results (dark dots), and the fragility functions used for the calibration of the discriminant functions (solid line). (b) Scatter plot of destroyed (red dots) and non-destroyed buildings (blue dots) according to the final discriminant function.

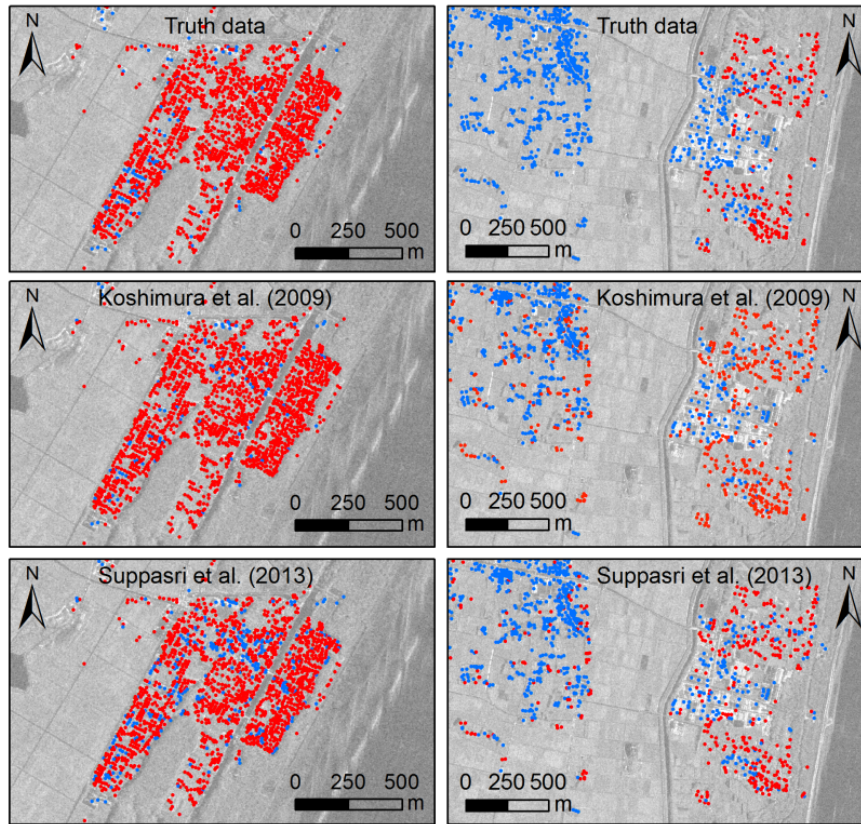


Fig. 4 – A closer look of the destroyed building map constructed from truth data and the proposed method.

### 3. Logistic regression-based upgrade of the damage mapping method

#### 3.1 Logistic regression classifier

A logistic regression classifier uses, as the name suggests, the logistic regression function to assign a label  $z_i \in \{0,1\}$  to a sample  $i$  that is associated with a set of features stored in the vector  $\mathbf{x}_i$ :

$$Pr(z_i = 1|\mathbf{x}_i) = h_{\theta, \theta_0}(\mathbf{x}_i) = \frac{1}{1 + \exp(-\boldsymbol{\theta}^T \mathbf{x}_i - \theta_0)} \quad (1)$$

where  $\mathbf{x} = (x_1, x_2, \dots, x_m)$  is a vector that contains the features of a sample (building),  $\boldsymbol{\theta} = (\theta_1, \theta_2, \dots, \theta_m)$  is a vector with the regression coefficients,  $\theta_0$  is an intercept term, and  $Pr(z_i = 1|\mathbf{x}_i)$  denotes the probability that  $z_i = 1$ , given the feature vector  $\mathbf{x}_i$ . The discriminant function is then defined as:

$$f(\mathbf{x}_i) = z_i = \begin{cases} 0 & \text{if } h_{\theta, \theta_0}(\mathbf{x}_i) < 0.5 \\ 1 & \text{if } h_{\theta, \theta_0}(\mathbf{x}_i) \geq 0.5 \end{cases} \quad (2)$$

Note that the hyperplane  $\boldsymbol{\theta}^T \mathbf{x}_i + \theta_0 = 0$  defines a boundary that separates the vectors  $\mathbf{x}_i$  with different labels. The unknowns  $\boldsymbol{\theta}$  and  $\theta_0$  are calibrated using training samples in the following optimization problem:

$$\min_{\boldsymbol{\theta}, \theta_0} (J(\boldsymbol{\theta}, \theta_0)) \quad (4)$$

$$J(\boldsymbol{\theta}, \theta_0) = -\frac{1}{N} \sum_{i=1}^N \left( \bar{z}_i \ln(h_{\theta, \theta_0}(\mathbf{x}_i)) + (1 - \bar{z}_i) \ln(1 - h_{\theta, \theta_0}(\mathbf{x}_i)) \right) \quad (5)$$

where  $N$  denotes the number of training samples. Note that the truth label of the training samples is assigned as  $\bar{z}_i$  in Eq. (5) in order to differentiate it from the label assigned from the discriminant function.

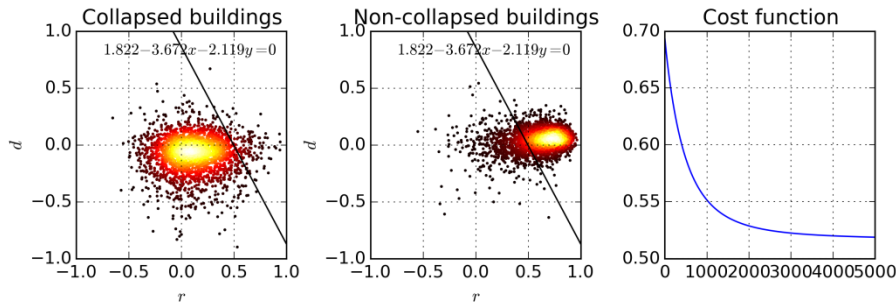


Fig. 5 – Linear discriminant function obtained using the fragility function of Koshimura et al. [33]. Left: scatter plot of the bi-dimensional samples that were destroyed by the tsunami. Center: scatter plot of the bi-dimensional data that were not destroyed by the tsunami. Right: Variation of the cost function,  $J(\boldsymbol{\theta}, \theta_0)$ , through the iterative gradient descent algorithm.

### 3.2 Upgrade of the damage mapping procedure

Although the procedure shown in Chapter 2 was proved to be effective for damage mapping, it exhibits important limitations. For instance, the parameters of the discriminant function were computed from an exhaustive search by constantly repeating steps (3)-(5) of Fig. 1. Such an approach is indeed not practical when the space dimension is larger than 2. Therefore, a modification of the logistic regression classifier was adapted to solve the referred issue.

Recall that  $\bar{z}_i$  is either 1, for damaged buildings, or 0, for non-damaged buildings. Accordingly, one of the two-terms in the summation of Eq. (5) always cancels for each training sample. Therefore, the contribution of a training sample to the function  $J(\boldsymbol{\theta}, \theta_0)$  is either  $\ln(h_{\boldsymbol{\theta}, \theta_0}(\mathbf{x}_i))$  or  $\ln(1 - h_{\boldsymbol{\theta}, \theta_0}(\mathbf{x}_i))$ . Recall also that our target is to avoid the use of training data. Thus, our modification consists of using unlabeled samples that will contribute to the summation of Eq. (5) with the both terms,  $\ln(h_{\boldsymbol{\theta}, \theta_0}(\mathbf{x}_i))$  and  $\ln(1 - h_{\boldsymbol{\theta}, \theta_0}(\mathbf{x}_i))$ ; however, each term will be weighted in the following form:

$$J(\boldsymbol{\theta}, \theta_0) = -\frac{1}{N} \sum_{i=1}^N \left( p_i \ln(h_{\boldsymbol{\theta}, \theta_0}(\mathbf{x}_i)) + (1 - p_i) \ln(1 - h_{\boldsymbol{\theta}, \theta_0}(\mathbf{x}_i)) \right) \quad (6)$$

where  $p_i$  and  $(1 - p_i)$  are the weight factors. The factor  $p_i$  is computed from a fragility function using the demand  $d_i$  that the sample  $i$  experienced. Using the Logistic Regression with the proposed modification, we were able to calibrate a discriminant function for  $n$ -dimensional space. In addition, optimization techniques, such as the gradient descent algorithm, can be used to solve Eq. (6). Fig. 5 illustrates the discriminant function resulted from the solution of Eq. (6) for the same case shown in Chapter 2, the 2011 Tohoku-Oki earthquake-tsunami. The results achieved an overall accuracy of 82.2% and 87.5% using the fragility functions provided by Koshimura et al. [33] and Suppasri et al. [34], respectively. The reader can find more detail of this work in [32].

## 4. Current works

Our modification of the Logistic Regression can be successfully applied only if fragility functions and demand parameters are available. The kind of disasters that fulfill this requirement are only earthquakes and tsunamis. In our current work, we are trying to implement methods that calibrate discriminant functions only from the estimation of the demand parameter. That is to say, fragility functions will not be necessary. With this new definition of the problem, the new methods can be applied to other type of disasters, such as floods and landslides. It is our belief that is still possible if we assume that a subset of samples whose demand



parameter is considerably low is composed of only non-damaged buildings. Then the main problem is to set a discriminant function that assigns a damaged state to a second subset of samples composed of samples with moderate/large demand parameters.

## 5. Conclusions

We reported two methods for damage mapping that can be implemented to work fully automatic. We have demonstrated that the training data used to calibrate supervised machine learning algorithms can be replaced with fragility functions and demand parameter maps. Fragility functions have been developed for decades, and currently are available in many countries for almost every material. The demand parameter map can also be computed from sensor instrumentation and numerical modeling. The method can overcome the difficulties encountered in supervised machine learning techniques while maintaining some of their advantages (i.e., the capacity to adapt to n-dimensional problems and the possibility of using nonlinear discriminant functions). The methods, however, can be applied only to earthquakes and tsunamis. Therefore, in our current work, we focus on a new definition of the problem, from which we are relaxing the constraints by using only the demand parameter map (i.e., fragility functions will no longer be a part of the constraints). The solution of the new problem will provide a damage mapping method that can be applied to other kinds of disasters, such as floods and landslides.

## 6. Acknowledgements

This study was partly funded by the J-Rapid project number JPMJRR1803; The JST CREST project number JP-MJCR1411; the JSPS Kakenhi Program project number 17H06108; and the National Fund for Scientific, Technological and Technological Innovation Development (Fondecyt – Peru) within the framework of the “Project for the Improvement and Extension of the Services of the National System of Science, Technology and Technological Innovation” (contract number 038-2019).

## 7. References

- [1] Kouchi K, Yamazaki F (2007): Characteristics of tsunami-affected areas in moderate-resolution satellite images. *IEEE Transactions on Geoscience and Remote Sensing*, **45**, 1650-1657.
- [2] Yamazaki F, Matsuoka M (2007): Remote sensing technologies in post-disaster damage assessment. *Journal of Earthquake and Tsunami*, **1**(3), 193-210.
- [3] Matsuoka M, Yamazaki F (2010): Comparative analysis for detecting areas with building damage from several destructive earthquakes using satellite synthetic aperture radar images. *Journal of Applied Remote Sensing*, **4**, 4-15.
- [4] Liu W, Yamazaki F, Gokon H, Koshimura S (2013): Extraction of tsunami-flooded areas and damaged buildings in the 2011 Tohoku-Oki earthquake from TerraSAR-X intensity images. *Earthquake Spectra*, **29**(S1), S183-S200.
- [5] Gokon H, Koshimura S, Matsuoka M (2016): Object-based method for estimating tsunami-induced damage using TerraSAR-X data. *Journal of Disaster Research*, **11** (2), 225-235.
- [6] Gokon H, Koshimura S, Meguro K (2017): Verification of a method for estimating building damage in extensive tsunami affected areas using L-band SAR data. *Journal of Disaster Research*, **12** (2), 251-258.
- [7] Liu W, Yamazaki F (2017): Extraction of collapsed buildings in the 2016 Kumamoto earthquake using multi-temporal PALSAR-2 data. *Journal of Disaster Research*, **12** (2), 241-250.
- [8] Karimzadeh S, Matsuoka M (2017): Building damage assessment using multisensory dual-polarized synthetic aperture radar data for the 2016 M 6.2 amatrice Earthquake, Italy. *Remote Sensing*, **9** (4), 17 pages.
- [9] Karimzadeh S, Matsuoka M (2018): Building damage characterization for the 2016 Amatrice earthquake using ascending-descending COSMO-SkyMed data and topographic position index. *IEEE Journal of Selected Topics in Applied Earth Observations and Remote Sensing*, **11** (8), 2668-2682.



- [10] Wieland M, Liu W, Yamazaki F (2016): Learning change from synthetic aperture radar images: Performance evaluation of a support vector machine to detect earthquake and tsunami-induced changes. *Remote Sensing*, **8** (10), 241-250.
- [11] Bai Y, Gao C, Singh S, Koch M, Adriano B, Mas E, Koshimura S (2018): A framework of rapid regional tsunami damage recognition from post-event TerraSAR-X imagery using deep neural networks. *IEEE Geoscience and Remote Sensing Letters*, **15**, 43-47.
- [12] Moya L, Yamazaki F, Liu W, Yamada M (2018): Detection of collapsed buildings from lidar data due to the 2016 Kumamoto earthquake in Japan. *Natural Hazard and Earth System Sciences*, **18** (1), 65-78.
- [13] Moya L, Zakeri H, Yamazaki F, Liu W, Mas E, Koshimura S (2019): 3D gray level co-occurrence matrix and its application to identifying collapsed buildings. *ISPRS Journal of Photogrammetry and Remote Sensing*, **149**, 14-28.
- [14] Moya L, Endo Y, Okada G, Koshimura S, Mas E (2019): Drawback in the change detection approach: false detection during the 2018 western Japan floods. *Remote Sensing*, **11**, 19 pages.
- [15] Geiß C, Pelizari PA, Blickensdrfer L, Taubenböck H (2019): Virtual support vector machines with self-learning strategy for classification of multispectral remote sensing imagery. *ISPRS Journal of Photogrammetry and Remote Sensing*, 151, 42-58.
- [16] Geiß C, Thoma M, Pittore M, Wieland M, Dech SW, Taubenböck H (2017): Multitask active learning for characterization of built environments with multisensory earth observation data. *IEEE Journal of Selected Topics in Applied Earth Observations and Remote Sensing*, 10 (12), 5583-5597.
- [17] Geiß C, Thoma M, Taubenböck H (2018): Cost-sensitive multitask active learning for characterization of urban environments with remote sensing. *IEEE Geoscience and Remote Sensing Letters*, 15 (6), 922-926.
- [18] Yamazaki F, Murao O (2000): Vulnerability functions for Japanese buildings based on damage data from the 1995 Kobe earthquake. In *Implications of Recent Earthquakes on Seismic Risk*. Imperial College Press, 91-102.
- [19] Karim KR, Yamazaki F (2003): A simplified method of constructing fragility curves for highway bridges. *Earthquake Engineering and Structural Dynamics*, 32 (10), 1603-1626.
- [20] Horie K, Hayashi H, Okimura T, Tanaka S, Maki N, Torii N (2004): Development of seismic risk assessment method reflecting building damage levels – Fragility functions for complete collapse of wooden buildings. *13th World Conference on Earthquake Engineering*, Vancouver, B. C., Canada.
- [21] Porter K, Kennedy R, Bachman R (2007): Creating fragility functions for performance-based earthquake engineering. *Earthquake Spectra*, **23** (2), 471-489.
- [22] Zülfikar AC, Fercan NOZ, Tunç S, Erdik M (2017): Real-time earthquake shake, damage, and loss mapping for Istanbul metropolitan area. *Earth, Planets and Space*, **69** (9), 15 pages.
- [23] Frolova NI, Larionov VI, Bonnin J, Sushchev SP, Ugarov AN, Kozlov MA (2017): Seismic risk assessment and mapping at different levels. *Natural Hazards*, **88** (1), 43-62.
- [24] Karimzadeh S, Feizizadeh B, Matsuoka M (2017): From GIS-based hybrid site condition map to an earthquake damage assessment in Iran: Methods and trends. *International Journal of Disaster Risk Reduction*, **22**, 23-36.
- [25] Geiß C, Pelizari PA, Marconcini W, Sengara W, Edwards M, Lakes T, Taubenböck H (2015): Estimation of seismic building structural types using multi-sensor remote sensing and machine learning techniques. *ISPRS Journal of Photogrammetry and Remote Sensing*, **104**, 175-188.
- [26] Shabestari KT, Yamazaki F (2003): Near-fault spatial variation in strong ground motion due to rupture directivity and hanging wall effects from the Chi-Chi Taiwan earthquake. *Earthquake Engineering and Structural Dynamics*, **32** (14), 2197-2219.
- [27] Kato T, Terada Y, Nishimura H, Nagai T, Koshimura S (2011): Tsunami records due to the 2010 Chile earthquake observed by GPS buoys established along the Pacific coast of Japan. *Earth Planets Space*, **63**, e5-e8.
- [28] Ozawa S, Nishimura T, Suito H, Kobayashi T, Tobita M, Imakire T (2011): Coseismic and postseismic slip of the 2011 magnitude-9 Tohoku-Oki earthquake. *Nature*, **471**, 373-376.



- [29] Matsuoka M, Yamamoto N (2012): Web-based quick estimation system of strong ground motion maps using engineering geomorphologic classification map and observed seismic records. *15th World Conference on Earthquake Engineering*, Lisbon, Portugal.
- [30] Irikura K, Miyakoshi K, Kamae K, Yoshida K, Somei K, Kurahashi S, Miyake H (2017): Applicability of source scaling relations for crustal earthquakes to estimation of the ground motions of the 2016 Kumamoto earthquake. *Earth Planets Space*, **69** (10), 13 pages.
- [31] Moya L, Mas E, Adriano B, Koshimura S, Yamazaki F, Liu W (2018): An integrated method to extract collapsed buildings from satellite imagery, hazard distribution and fragility curves. *International Journal of Disaster Risk Reduction*, **31**, 1374-1384.
- [32] Moya L, Marval-Perez LR, Mas E, Adriano B, Koshimura S (2018): Novel unsupervised classification of collapsed buildings using satellite imagery, hazard scenarios and fragility functions. *Remote Sensing*, **10**, 16 pages.
- [33] Koshimura S, Oie T, Yanagisawa H, Imamura F (2009) Developing fragility functions for tsunami damage estimation using numerical model and post-tsunami data from Banda Aceh, Indonesia. *Coastal Engineering Journal*, **51** (3), 243-273.
- [34] Suppasri A, Mas E, Charvet I, Gunasekera R, Imai K, Fukutani Y, Abe Y, Imamura F (2013): Building damage characteristics based on surveyed data and fragility curves of the 2011 Great East Japan tsunami, *Natural Hazards*, **66** (2), 319-341.